SSRG International Journal of Electrical and Electronics Engineering
ISSN: 2348-8379/ https://doi.org/10.14445/23488379/IJEEE-V13I8P111

Volume 13 Issue 8, 126-140, August 2026

Original Article

Beam Reconfigurable Antenna Integrated with Passive Transmissive FSS Superstrate for Beam-Tilt Enhancement

Rabiatuladawiah Akhbar[1], Hajar Ja'afar[2*], Nurul Huda Abd Rahman[3], Nurulazlina Ramli[4], Mohamed Nasrun Osman[5], Rina Abdullah[6]

[1]*Centre of Foundation Studies, Universiti Teknologi MARA, Cawangan Selangor, Dengkil Campus, 43800 Dengkil, Selangor, Malaysia.*
[2]*Faculty of Electrical Engineering, Universiti Teknologi MARA, Cawangan Johor, Pasir Gudang Campus, 81750 Masai, Johor, Malaysia.*
[3]*Antenna Research Centre, Faculty of Electrical Engineering, Universiti Teknologi MARA, 40450 Shah Alam, Selangor, Malaysia.*
[4]*Centre for Advanced Electrical and Electronic System, SEGi Universiti, Selangor, Malaysia.*
[5]*Faculty of Electronic Engineering and Technology, Universiti Malaysia Perlis, Kampus Pauh Putra, 02600 Arau Perlis, Malaysia.*
[6]*Faculty of Electrical Engineering, Universiti Teknologi MARA,2300 Dungun, Terengganu, Malaysia.*

[*]*Corresponding Author : hajarj422@uitm.edu.my*

Received: 22 May 2026 Revised: 20 July 2026 Accepted: 10 August 2026 Published: 25 August 2026

Abstract *- This work presents a 360° beam reconfigurable circular patch antenna integrated with a passive transmissive Frequency Selective Surface (FSS) to enhanced beam tilt performance at 3.5 GHz. The baseline antenna achieved full azimuthal coverage, but the beam tilt is limited to approximately ±24°-29° due to restricted phase gradient control by the parasitic elements. To overcome this beam tilt limitation, a nested-square transmissive FSS superstrate is introduced as a passive superstrate to reinforce the existing phase gradient and increase the beam tilt angle of the antenna. The optimized FSS unit cell provides high transmission (|S21| = -0.13 dB) and low reflection (|S11| = -40 dB) at the operating frequency. Parametric studies identify a 1×4 array positioned 8 mm above the antenna as the optimum configuration, resulting tilt enhancement to ±32°-34°, improved sidelobe levels (-6 to -7 dB), and stable gain (≈ 6.7-7.9 dBi). A prototype was fabricated and validated in an anechoic chamber, with close agreement observed between simulated and measured beam tilt angle, gain, HPBW, S11 and efficiency (> 87%). These results demonstrate that a passive transmissive FSS can reinforce parasitic-induced phase gradients and provide a compact, low-loss solution for sub-6 GHz 5G beam-tilting applications.*

Keywords *- Reconfigurable antenna, Transmissive FSS, Beam tilting, FSS superstrate, Sub-6 Ghz 5g systems.*

1. Introduction

Reconfigurable antennas have emerged as a key enabling technology for modern wireless systems due to their ability to modify their electromagnetic characteristics after fabrication. Depending on the antenna structure and reconfiguration mechanism, parameters such as operating frequency [1, 2], radiation pattern [3, 4], polarization [5] can be controlled individually or in any combination [6].

Reconfigurable antennas can provide beam scanning capability, improved link reliability and enhanced spectral efficiency, while maintaining a compact and low-cost implementation. Among the different types of reconfigurable antennas, pattern-reconfigurable or beam steering antennas are particularly attractive for wireless communication systems because they can direct the radiated energy toward the selected angular regions and reduce interference in undesired directions [3, 4].

Beam steering can be achieved using various techniques, including phased arrays [7-9], pixel-based reconfigurable apertures [10-15] and switched parasitic elements inspired by the Yagi-Uda concept [16-19]. Although these methods can redirect the radiation pattern, their implementation commonly involves a trade-off among steering range, antenna size, circuit complexity, power consumption and radiation performance. Phased array and pixel-based approaches can provide flexible beam control but generally require multiple phase shifters and active control components. In contrast, parasitic-element antennas offer a simpler switching structure, although their beam tilt capability is often restricted by the relatively weak phase variation produced through mutual coupling.

Although beam steering can be realized using phased arrays, pixel-based antennas, parasitic-element antennas and active electromagnetic surfaces, these approaches generally involve trade-offs between steering performance, structural complexity and implementation cost.

Therefore, there remains a need for a compact and low complexity solution capable of improving beam tilt performance without introducing additional active control circuits. Based on the reviewed literature, limited experimental work has investigated the use of a passive transmissive FSS specifically to reinforce the phase gradient generated by switchable parasitic elements.

To address this gap, the present work integrates a passive transmissive FSS superstrate with a beam reconfigurable circular patch antenna operating at 3.5 GHz. The antenna is made up of six hexagon-shaped circular parasitic elements surrounding a circular driven patch.

Each parasitic element is controlled using an RF p-i-n diode, allowing the surrounding elements to operate as directors or reflectors under different switching conditions. The parasitic element antenna provides six beam tilted configurations covering different azimuthal sectors and two broadside configurations. However, the beam tilted configurations of the antenna without FSS are limited to approximately ±24°-29°.

A compact 1×4 transmissive FSS composed of nested square unit cells is positioned above the antenna to modify the transmitted field distribution. Unlike active FSS structures or reconfigurable surfaces that require additional switching and biasing circuits, the proposed FSS operates passively in a low reflection transmission region. Its function is to reinforce the phase variation initially produced by the switched parasitic elements rather than to generate an independently controlled phase distribution. With the optimized FSS aperture and an 8 mm air gap height, the measured beam tilt angle range is increased to approximately ±32°-34° without introducing additional active components or modifying the original switching configurations.

The main contributions of this work are the development of a six parasitic element circular patch antenna capable of 360° azimuthal sector switching, the design of a low reflection transmissive FSS unit cell at 3.5 GHz, the systematic optimization of the FSS aperture length and antenna-FSS separation and the experimental demonstration that a passive transmissive FSS can increase the parasitic element induced beam tilt angle without introducing an additional FSS biasing circuit.

Section 2 analyzes the existing beam steering antenna techniques and identifies the research gap addressed in this work. Section 3 presents the antenna structure, switching configuration and operating principle of the proposed parasitic-via reconfigurable circular patch antenna. Section 4 describes the design of the transmissive FSS unit cell and its parametric optimization. Section 5 investigates the integration of the FSS with the reconfigurable antenna, including the effects of the FSS aperture length and antenna-FSS air gap height to the antenna radiation characteristics. Section 6 presents the validation through measurement results. Finally, Section 7 summarized the main findings and highlights its suitability for compact sub-6 GHz 5G beam-steering applications.

2. Literature Review

Phased arrays are widely used for electronic beam steering because the beam direction can be controlled by adjusting the relative excitation phases of the antenna elements [7]. These arrays can provide high gain and steer the beam over a wide angular range [7-9]. However, conventional phased arrays require multiple phase shifters and control components, which increased power consumption, cost and hardware complexity, particularly when a large number of elements is used [7].

Pixel antennas and reconfigurable apertures divide the radiating surface into many electrically small pixels connected by RF switches [10-15]. Different combinations of connected and disconnected pixels modify the effective current paths, allowing the antenna to produce several radiation patterns and beam directions. These antennas offer considerable pattern flexibility and may provide a large number of reconfiguration states. However, their implementation can require many switches, bias lines and possible connection states, resulting in increased complexity [10, 11, 13-15].

Parasitic element beam reconfigurable antennas provide a more hardware-efficient alternative because only the driven element is directly excited. The surrounding parasitic elements interact with the driven radiator through mutual coupling and can be configured to operate as directors or reflectors [16-19]. By controlling the electrical states of the parasitic elements using RF p-i-n diodes or other RF switches, an asymmetric surface current distribution is established around the driven element. This creates a lateral phase gradient across the antenna aperture, steering the main beam toward selected angular sectors without requiring a separate phase shifter for each radiating element.

Although parasitic element antennas have relatively simple feeding structures, their performance depends strongly on the arrangement of the parasitic elements, the effective aperture, the ground plane configuration and the switching network. Moderate beam tilt angles can be obtained using compact planar parasitic structures, while larger steering ranges extending toward the endfire direction have been demonstrated using additional parasitic layers, partial ground planes or a larger number of switching components [16-19]. Consequently, a trade-off remains among the beam steering range, antenna profile, number of switches, gain consistency and biasing complexity.

Frequency-Selective Surfaces (FSS) are periodic structures designed to manipulate the transmission and reflection of electromagnetic waves over a selected frequency range. Passive FSS structures are commonly integrated with antennas as superstrates for filtering, gain enhancement and wavefront modification.

Their electromagnetic response is determined by the geometry, material properties and arrangement of the unit cells. A passive FSS can also influence the beam direction when it introduces a non-uniform transmission phase across the effective antenna aperture. However, because no tunable component is incorporated into the unit cells, its response remains fixed after fabrication.

Active FSS structures incorporate tunable components such as an RF p-i-n diode or varactor diode into their unit cells. By controlling the states of these components, the transmission or reflection phase of different FSS regions can be varied electronically, allowing the FSS to generate the phase gradient required for beam steering [20-22]. An active transmissive FSS integrated with a horn antenna achieved beam steering of ±30° across a multilayer FSS [20].

A reconfigurable FSS-based PRS antenna produced a beam tilted of ±22° with a realized gain of 10 dBi [21]. Although these active FSS structures provide direct electronic control over beam direction, they require additional active components and biasing circuits, which increase the overall design complexity and may introduce additional losses.

Table 1. Comparative analysis of recently reported beam-steering antenna

Ref.	Technique	Maximum Beam Tilt angle (°)	Gain (dBi)	Active Control	Key Limitation
[12]	Reconfigurable parasitic pixel layer	±40°	~8.0	Yes	Multiple switches and a large aperture
[18]	Parasitic array	±30°	4.9-6.5	Yes	Moderate tilt angle and non-uniform gain
[20]	Active transmissive FSS	±30°	12.2-15.4	Yes	Five FSS layer and insertion loss
[21]	Reconfigurable PRS	±22°	~10	Yes	72-pin diodes and biasing complexity
[22]	Active FSS	±32°	~7.28	Yes	64-pin diode and biasing complexity
This work	Parasitic patch + passive transmissive FSS	±34°	~7.98	No additional FSS control	Discrete steering states

As summarized in Table 1, previous studies have proposed various beam steering antenna designs based on reconfigurable parasitic pixel antennas, switchable parasitic element antennas, active transmissive FSS structures and reconfigurable PRS antennas. In contrast, the present work enhances the beam tilt performance of an existing switchable parasitic element antenna by integrating a passive transmissive FSS superstrate. The switchable parasitic elements establish the initial beam direction by generating a lateral phase gradient across the antenna aperture, while the passive FSS modifies the transmitted phase distribution to reinforce this existing phase gradient. As a result, the beam tilt angle is increased from approximately ±24°-29° to ±32°-34° without modifying the original switching configuration or introducing additional active components and biasing circuits into the FSS.

3. Antenna Design and Configuration

3.1. Antenna Structure

The proposed beam reconfigurable antenna was designed and optimized using CST Microwave Studio. The baseline antenna consists of a circular microstrip patch etched on a Rogers RT5880 substrate with a thickness of 1.575 mm, a relative permittivity $\varepsilon r = 2.2$ and a loss tangent $\tan \delta = 0.0019$.

The substrate uses a full copper ground plane on its bottom side. The circular Driven Element (DE) is excited by a coaxial probe feed from the bottom of the substrate, as shown in Figure 1.

The feed position is offset from the patch center and optimized to achieve a 50 Ω input impedance at a frequency of 3.5 GHz. The resonant frequency of the circular patch is primarily governed by its radius, which is determined using the well-known microstrip circular patch design equations [23]. Based on these relations, the radius of the driven patch is selected as r = 15.96 mm to obtain resonance at 3.5 GHz.

To realize beam reconfigurability, six identical circular parasitic elements are then placed symmetrically around the driven patch in a hexagonal arrangement for balance mutual coupling, each separated by a uniform gap g = 3 mm from the driven element. These parasitic elements are denoted as PE A, PE B, PE C, PE D, PE E and PE F and are spaced by 60° in the azimuth plane to cover the full 360° angular range.

The radius of each parasitic patch, rp, is chosen slightly smaller than the driven patch (rp = 0.99r) to ensure strong but controlled mutual coupling.

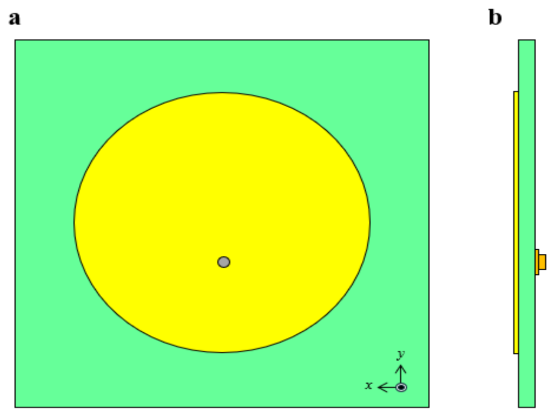

Fig. 1 Initial antenna structure (a) Front view, and (b) Side view.

Each parasitic element is embedded with an RF p-i-n diode (D1-D6) and connected to the ground plane through a shorting via with a diameter of a = 1.2 mm. The shorting via is positioned at an optimized location on each parasitic element to control the current path and mutual coupling between the driven and parasitic elements. The position of shorting via is an important design parameter because it directly influences the surface current distribution on the parasitic elements. As a result, the phase gradient across the antenna aperture affects the achievable beam tilt angle. The overall substrate dimensions are Ws × Ls = 120 mm × 120 mm (1.4 λo × 1.4 λo). As depicted in Figure 2 is the overall structure of beam reconfigurable antenna. This structure forms the foundation for the subsequent integration with the transmissive FSS superstrate. The final optimized dimensions of the proposed parasitic-via hexagonal circular patch antenna are summarized in Table 2.

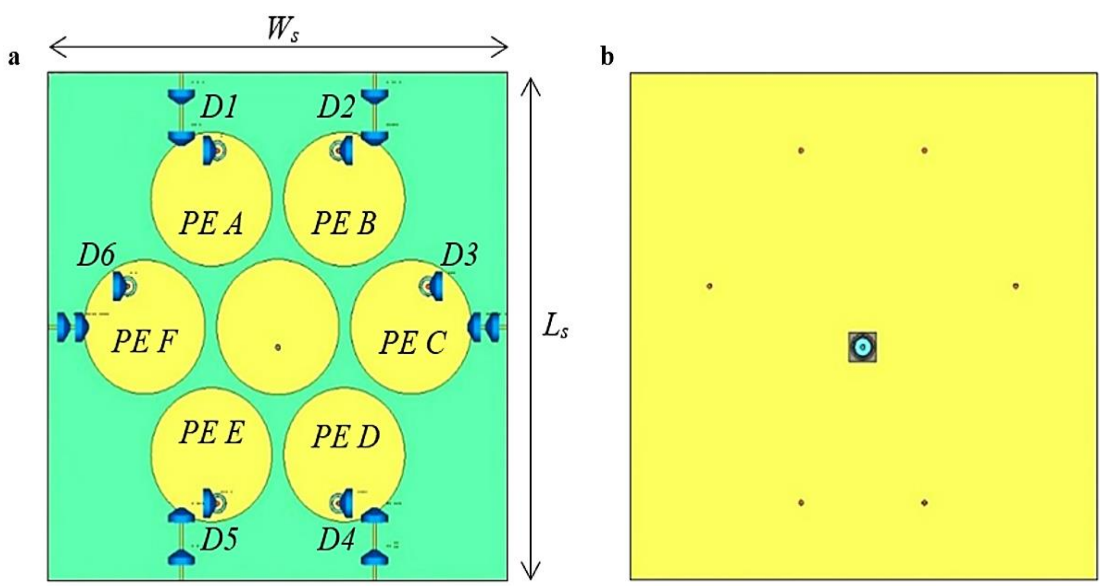

Fig. 2 Reconfigurable antenna structure, (a) Front view, and (b) Side view.

Table 2. Optimized parameters of the reconfigurable antenna

Parameter	Value (mm)	Parameter	Value (mm)
Width of substrate, Ws	120	Radius of parasitic, rp	0.99*r
Length of substrate, Ls	120	Gap between the driven and parasitic patch	3
Radius of patch, r	15.96	Diameter of shorting vias, a	1.2

3.2. Antenna Working Principle

The radiation characteristic of the proposed antenna is controlled by the mutual coupling established between the driven circular patch and its surrounding parasitic elements. When a parasitic element is electrically connected to the ground plane through a shorting via and the RF p-i-n diode is forward biased (ON state), it acts as a reflector. As a result, the induced surface current redirects the radiated energy away from the reflector, thereby steering the main beam toward the opposite direction. In contrast, when the RF p-i-n diode is reverse biased (OFF state), and the connection to the ground plane is removed, allowing the parasitic element acts as a director. Consequently, the induced surface current redirects the radiated energy toward the director, steering the main beam in its direction. By selectively configuring the surrounding parasitic element as a director or reflector, an asymmetric current distribution is generated around the driven patch, resulting in a corresponding near-field phase distribution that redirects the main beam toward the region dominated by director elements.

In the CST simulation model, the shorting vias are implemented as metallic (copper) pins representing the ON state and as vacuum cylinders representing the OFF state to prove the concept of reconfigurable. The RF p-i-n diodes (MACOM MADP-000907-14020) are modeled using Touchstone (S-parameter) blocks that capture their frequency-dependent behavior in both forward-biased (ON) and reverse-biased (OFF) conditions. The diodes are placed in narrow circular slots (0.7 mm wide) etched in the parasitic patches to provide DC isolation between the RF and bias networks.

The anode of each diode is linked to a small circular pad connected to the ground plane through the shorting via, while the cathode is connected to the main body of the parasitic patch through a bias line. Inductors, L of 27 nH, are employed as RF chokes, allowing DC current to bias the diodes while blocking RF leakage into the bias lines. The diodes are biased with 0 V reverse bias to realize a low OFF capacitance of approximately 0.025 pF.

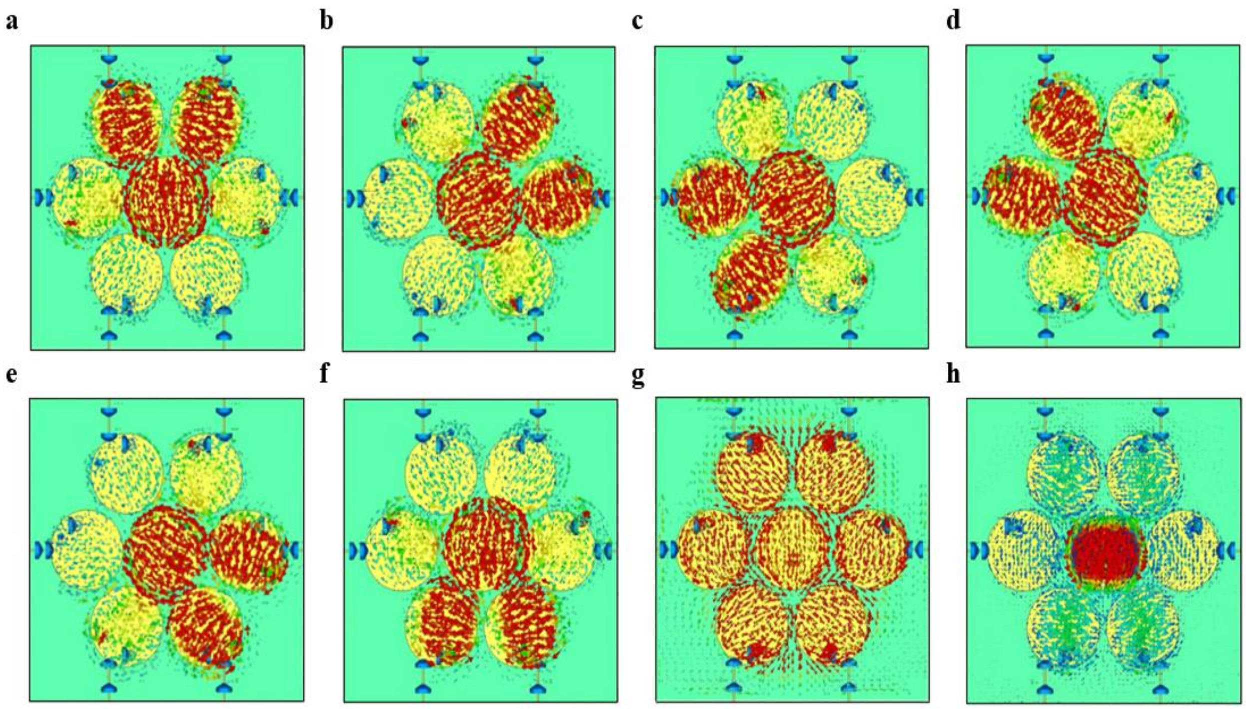

Fig. 3 Current distribution for switching configuration: (a) A1, (b) A2, (c) A3, (d) A4, (e) A5, (f) A6, (g) A7, and (h) A8.

To systematically investigate the beam reconfiguration capability of the proposed antenna, eight switching configurations (A1-A8) are defined. In modes A1-A6, two adjacent parasitic elements are configured in the OFF state (directors), while the remaining four are in the ON state (reflectors).

This asymmetric director-reflector configuration creates a non-uniform current distribution around the driven patch, generating a lateral near-field phase gradient that steers the main beam toward the director pair. Consequently, a tilted beam is produced in the corresponding azimuth direction. In modes A7 and A8, all parasitic elements are operates as directors (all OFF) and reflectors (all ON) respectively, resulting in broadside radiation with different gain and beamwidth characteristics.

The simulated surface current distributions for modes A1-A8, shown in Figure 3, confirm the director-reflector operation of the parasitic elements. In the beam tilted modes (A1-A6), strong surface current is concentrated on the OFF-state parasitic elements acting as directors, whereas the ON-state parasitic elements exhibit weaker currents due to the grounding effect introduced by the shorting vias. This controlled asymmetry in surface current distribution established a lateral phase gradient across the antenna aperture, steering the main beam toward the OFF-state parasitic pair. In mode A7 (all directors), strong currents are observed on all parasitic elements, forming a larger effective aperture that produces a narrow high-gain broadside beam. In contrast, mode A8 (all reflectors) suppresses the currents on the parasitic elements, causing radiation on the driven patch alone, which produces a wider low-gain broadside beam.

The corresponding beam tilt angle, gain, HPBW and Sidelobe Level (SLL) for each switching mode are summarized in Table 3. These results demonstrate that the proposed antenna achieves 360° azimuthal beam reconfigurability with beam tilt angles of up to ±29° prior to FSS integration. The effects of integrating the passive transmissive FSS are investigated in the following sections using these switching modes as the baseline for comparison.

Table 3. Simulated radiation characteristics of the proposed beam reconfigurable antenna for all switching configurations

Mode	Switching configuration						Tilted angle (°)	Gain (dB)	HPBW (°)	SLL (dB)
	D1	D2	D3	D4	D5	D6				
A1	OFF	OFF	ON	ON	ON	ON	24°	7.86	61.8°	-2.3
A2	ON	OFF	OFF	ON	ON	ON	29°	7.35	69.1°	-3.4
A3	ON	ON	OFF	OFF	ON	ON	29°	7.11	71.0°	-3.2
A4	ON	ON	ON	OFF	OFF	ON	-27°	7.95	60.0°	-2.2
A5	ON	ON	ON	ON	OFF	OFF	-29°	7.12	71.0°	-3.2
A6	OFF	ON	ON	ON	ON	OFF	-29°	7.34	69.5°	-3.5
A7	OFF	OFF	OFF	OFF	OFF	OFF	0°	10.2	33.9°	-6.4
A8	ON	ON	ON	ON	ON	ON	0°	7.42	90.5°	-

4. Passive Transmissive Frequency Selective Surface (FSS)

4.1. Design of Unit Cell

To enhance the beam tilt radiation of the proposed reconfigurable antenna, a passive transmissive Frequency-Selective Surface (FSS) is introduced as a passive superstrate. The FSS is designed to operate as a low-loss passband surface centered at 3.5 GHz, providing high transmission magnitude while preserving the phase response required for wavefront transformation. The FSS is implemented on a Rogers RT5880 substrate with $\varepsilon_r = 2.2$, $\tan\delta = 0.0019$ and a thickness of 1.575 mm, consistent with the antenna substrate for ease of fabrication and to avoid additional dielectric interfaces.

The design process begins with a single solid square metallic patch unit cell. To characterize its frequency-selective surface behaviour, periodic boundary conditions are applied so that the cell represents as an infinite periodic surface.

The infinite periodic surface is modeled in CST Microwave Studio using periodic boundary conditions and excited by a pair of Floquet ports under normal incidence to extract the transmission (S21) and reflection (S11) coefficients. The simulated response of this initial configuration exhibits a passband at a frequency higher than the target 3.5 GHz due to insufficient capacitive loading of the structure, as shown in Figure 4(a).

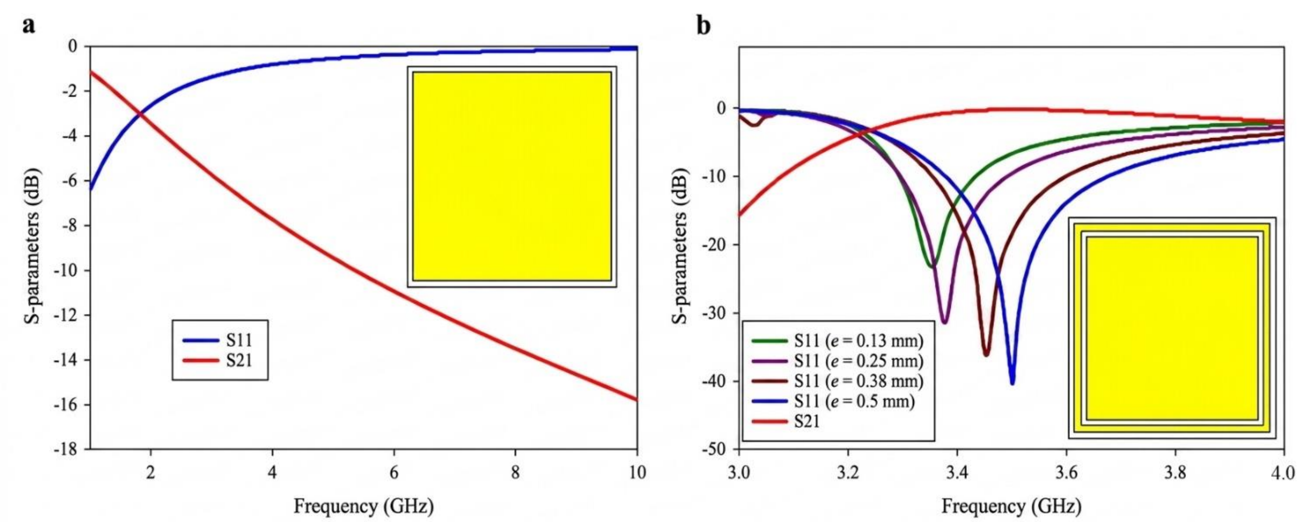

Fig. 4 Simulated reflection(|S11|) and transmission (|S21|) coefficients of the proposed transmissive FSS unit cells (a) Square metallic patch, and (b)Square patch with square slot.

To shift the resonance toward the desired band, a concentric square slot is introduced inside the metallic patch, forming a nested square-loop geometry as shown in Figure 4(b). The introduction of the slot increases the capacitive coupling between opposing metallic edges and effectively lengthens the current path. Consequently, the resonant frequency is reduced toward the required operating frequency. Electromagnetically, the nested square patch with a narrow slot behaves as a series LC resonant network. The metallic loop contributes an effective inductance L, while the narrow slot gap introduces an effective capacitance, C, between adjacent edges. The resonant frequency of the unit cell can therefore be approximated as:

$$f_r = \frac{1}{2\pi\sqrt{LC}} \quad (1)$$

indicating that increasing capacitance lowers the resonant frequency, whereas reducing capacitance shifts it upward. This equation guides the optimization of the FSS response in this work.

The aforementioned equation leads to selection of the slot-gap width e as the primary tuning parameter because it directly controls the capacitive coupling across the slot. A parametric sweep is carried out by varying e from 0.13 mm to 0.50 mm. When e is small, the close spacing of the metallic edges increases capacitance, causing the passband to shift to lower frequencies. In contrast, increasing e will lead to decreases capacitance causes the frequency to shift to higher frequency. As observed in Figure 4(b), the transmission peak gradually shifts from approximately 3.3 GHz to 3.5 GHz as e increases. The optimal value e = 0.15 mm aligns the passband precisely at the target frequency while maintaining very low reflection.

Table 4 summarizes the optimized parameters of the proposed unit cell, and the structure is shown in Figure 5(a). The transmission coefficient magnitude is |S21| ≈ -0.13 dB, indicating near unity transmission, while the reflection coefficient is |S11| ≈ -40.4 dB, indicating very low reflection at the target frequency of 3.5 GHz, as shown in Figure 5(b).

These results confirm that the proposed unit cell functions as an efficient transmissive FSS and is suitable to act as a passive superstrate for the integrated FSS-antenna structure analyzed in Section 5.

Table 4. Optimized parameters of the proposed unit cell

Parameter	Value (mm)
p_x	20
p_y	20
b	18.8
c	17.8
d	16.8
e	0.15

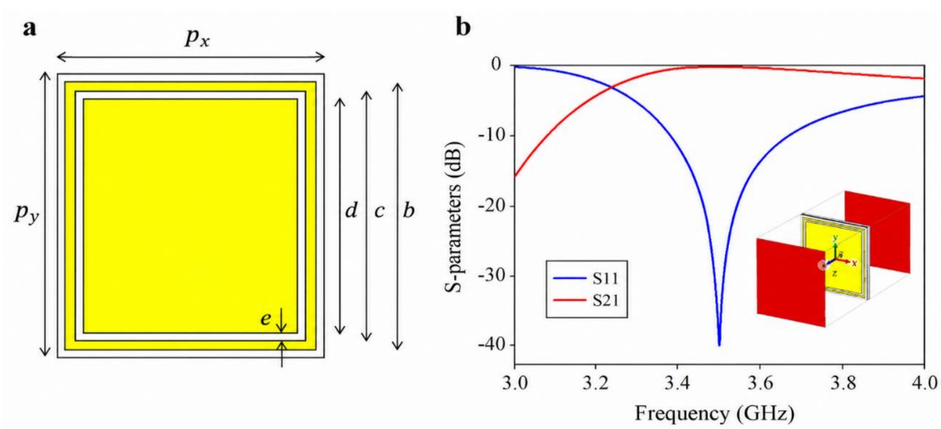

Fig. 5 Proposed passive transmissive FSS: (a) Geometry of the unit cell, and (b)Simulation setup and simulated reflection and transmission coefficients of the unit cell.

5. Integrated Passive Transmissive FSS with Proposed Beam Reconfigurable Antenna

The beam steering capability of parasitic-element reconfigurable antennas originates from the asymmetric near-field interaction between the circular patch and the surrounding parasitic elements. By selectively configuring the parasitic elements as directors and reflectors, an uneven surface current distribution is produced, which establishes a lateral phase imbalance across the antenna aperture and results in a tilted main beam. However, in parasitic-only configurations, the achievable beam tilt angle is fundamentally limited by the finite physical aperture and the relatively weak phase gradient that can be generated through mutual coupling alone, typically restricting the tilt to values below approximately 30°.

To solve this inherent beam tilt limitation, a transmissive Frequency-Selective Surface (FSS) is employed as a passive superstrate positioned above the antenna. Unlike reflective or partially reflective surfaces that rely on resonant cavity effects, the proposed FSS is designed to operate in a low-loss transmission regime, where its primary function is to manipulate the transmission phase distribution of the radiated wave. As a result, the FSS strengthens the phase gradient which is already imposed by the parasitic elements director-reflector configuration, enabling enhanced beam tilting and wavefront control while preserving the original antenna architecture.

The far-field beam direction of an aperture-type radiator can be related to the spatial phase distribution across the effective aperture. The beam-tilt angle θ along the steering axis can be expressed as:

$$\theta \approx \sin^{-1}\left(\frac{\lambda}{2\pi}\frac{d\phi(x)}{dx}\right) \quad (2)$$

where λ is the free space wavelength and $d(\phi)/dx$ represents the lateral phase gradient. In the proposed antenna, switching states of the parasitic elements establish an initial phase gradient around the driven patch. The transmissive FSS superstrate subsequently further modifies the transmitted phase distribution, resulting in a large phase variation across the effective aperture. Consequently, the radiated fields combine constructively in an off-broadside direction, producing enhanced beam steering and a larger beam-tilt angle. However, if the FSS aperture becomes excessively large or the antenna-FSS spacing is improperly selected, the resulting phase distribution may become non-uniform and lead to reduced steering stability.

Based on the operating principle of the proposed antenna-FSS configuration, two design parameters influence the beam tilt enhancement performance, which are the number of unit cells (1×N) and the air gap height, h, between the antenna and the FSS superstrate.

The FSS aperture determines the spatial extent of phase transformation, whereas the air gap height, h, controls the electromagnetic coupling strength and phase uniformity. To identify the optimum configuration, the influence of these two parameters on the beam steering performance is investigated in the following subsection.

5.1. Parametric Study of the Number of Unit Cells $(\mathbf{1 \times N})$ in FSS Integration

To determine the optimal spatial extent of the transmissive FSS, linear arrays consisting of N = 2-6 unit cells (1×N) were evaluated.

In all cases, the FSS was centered above the driven patch and aligned along the beam-steering axis to ensure that the transmission-phase modulation introduced by the FSS constructively reinforced the phase gradient generated by the parasitic element. The air-gap height was fixed at 8 mm during this study to isolate the effect of aperture length.

Table 5. Radiation characteristics of integrated FSS with reconfigurable antenna in terms of tilted angle and gain

Mode	Tilted angle (°)						Gain (dB)					
	Without FSS	1 × 2	1 × 3	1 × 4	1 × 5	1 × 6	Without FSS	1 × 2	1 × 3	1 × 4	1 × 5	1 × 6
A1	24°	32°	34°	32°	34°	31°	7.86	7.58	7.85	7.81	7.93	7.9
A2	29°	33°	4°	33°	29°	27°	7.35	6.7	6.39	7.2	7.44	6.99
A3	29°	33°	5°	34°	30°	28°	7.11	6.4	6.08	6.75	7.05	6.65
A4	-27°	-34°	-36°	-33°	-35°	-32°	7.95	7.74	8.01	7.98	8.15	8.33
A5	-29°	-33°	-5°	-34°	-30°	-28°	7.12	6.4	6.08	6.75	7.05	6.65
A6	-29°	-33°	-4°	-33°	-29°	-27°	7.34	6.7	6.39	7.2	7.44	6.99
A7	0°	0°	0°	0°	0°	0°	10.2	9.84	9.59	9.83	7.99	9.46
A8	0°	0°	0°	0°	0°	0°	7.42	6.01	5.88	6.29	7.11	7.04

For the parasitic-only antenna, the tilted-beam modes (A1-A6) exhibit beam angles in the range of ±24° to ±29°, reflecting the limited phase gradient achievable through parasitic coupling alone. With the introduction of the transmissive FSS, a clear enhancement in beam tilt angle is observed as the number of unit cells increases for most configurations, as tabulated in Table 5.

Among the investigated apertures, the 1×4 configuration FSS provides the most consistent performance across all steering modes. Specifically, the positive steering modes (A1-A3) achieve beam angles of approximately +32° to +34°, while the negative steering modes (A4-A6) reach -33° to -34°. Compared with the parasitic-only antenna, these results corresponding to a beam tilt enhancement of up to approximately 14%-42%, za depending on the configurations mode. Importantly, this increase in beam tilt angle is not accompanied by a significant degradation in gain. Across all FSS configurations, the realized gain of tilted modes for 1×4 FSS remains within the range of approximately 6.7-7.9 dBi, comparable to the baseline antenna.

As tabulated in Table 6, the integration of the FSS influences both the Half-Power Beamwidth (HPBW) and Sidelobe Level (SLL) of the reconfigurable antenna. For most steering modes, particularly A1, A2, A4, A6 and A7, HPBW remains relatively controlled, indicating that the FSS modifies the transmitted phase distribution without causing excessive main lobe broadening.

However, larger HPBW variations are observed in certain modes, especially for A3, A5 and A8 suggested that some FSS aperture sizes may introduce non-uniform phase distribution and reduce radiation pattern stability.

In terms of SLL, several modes exhibit noticeable improvement after FSS integration. For example, A2 and A6 show significant SLL reduction for the 1×3 configuration, while A3 and A5 exhibit improves SLL for both 1×3 and 1×5 configurations. The A7 mode also shows gradual SLL improvement as the FSS aperture increases, reaching its best value at the 1×5 configuration. Nevertheless, the improvement is not uniform across all modes, and some configurations show fluctuating SLL behavior, indicating that increasing the number of unit cells does not always result in more stable radiation performance.

When the FSS aperture is extended beyond four unit cells (1×5 and 1×6), the overall performance does not consistently improve. Although some modes configurations achieve better SLL or narrower HPBW, the radiation characteristics become less uniform across all operating modes.

This behavior can be attributed to increased phase nonlinearity and edge diffraction effects related to the enlarged finite FSS aperture, which disturb the desired quasi-linear phase distribution across the transmitted wavefront.

Table 6. Radiation characteristics of integrated FSS with reconfigurable antenna in terms of HPBW and SLL

Mode	Without FSS	HPBW (°)					Without FSS	SLL (dB)				
		1 × 2	1 × 3	1 × 4	1 × 5	1 × 6		1 × 2	1 × 3	1 × 4	1 × 5	1 × 6
A1	61.8°	62.6°	62.8°	62.5°	62.4°	64.1°	-2.3	-2.1	-2.1	-2.2	-1.2	-2.2
A2	69.1°	70.6°	74.6°	67.7°	55.3°	54.6°	-3.4	-3.6	-16.9	-7.1	-15.1	-7.1
A3	71.0°	72.0°	93.6°	66.2°	56.3°	64.6°	-3.2	-3.5	-10.8	-6.6	-14.0	-6.1
A4	60.0°	60.7°	60.4°	60.1°	59.7°	59.0°	-2.2	-2.2	-2.0	-2.1	-1.5	-2.4
A5	71.0°	71.9°	93.6°	66.2°	56.3°	64.6°	-3.2	-3.5	-10.8	-6.6	-14.0	-6.1
A6	69.5°	70.5°	74.6°	67.7°	55.3°	64.6°	-3.5	-3.6	-16.9	-7.1	-15.1	-7.1
A7	33.9°	35.1°	35.7°	35.9°	46.4°	36.6°	-6.4	-7.3	-7.8	-7.5	-10.2	-8.7
A8	90.5°	100.5°	89.9°	96.2°	69.6°	76.0°	-	-	-16.9	-	-16.6	-

Overall, the results demonstrate that the transmissive FSS acts as a passive phase-gradient reinforcement structure, but its effectiveness strongly depends on the number of unit cells forming the aperture. Among the investigated configurations, the 1×4 FSS, as shown in Figure 6, offers the most balanced performance by maintaining consistent beam tilt enhancement across all steering modes while preserving gain, HPBW, and acceptable SLL characteristics. Consequently, the 1×4 configuration is selected for further investigation in the subsequent air-gap parametric study.

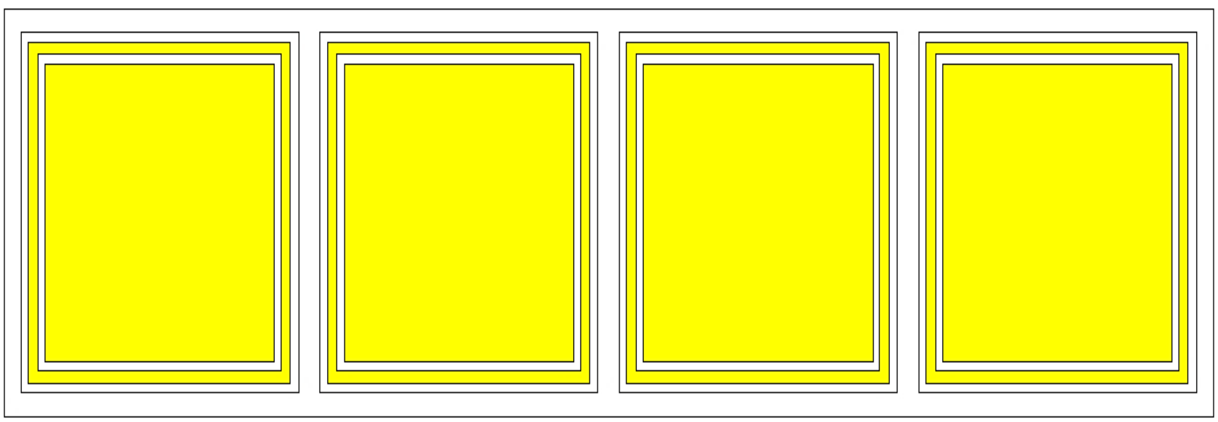

Fig. 6 1 × 4 Passive transmissive FSS array

5.2. Parametric Study of the Air Gap

The vertical separation between the transmissive 1×4 FSS array and the reconfigurable antenna, denoted as the air gap height h, as shown in Figure 7, plays an important role in determining the electromagnetic coupling strength and the uniformity of the phase transformation imposed by the FSS. To examine these effects, the air gap was varied from 6 mm to 12 mm in steps of 2 mm. The antenna performance was then evaluated for all switching modes (A1-A8).

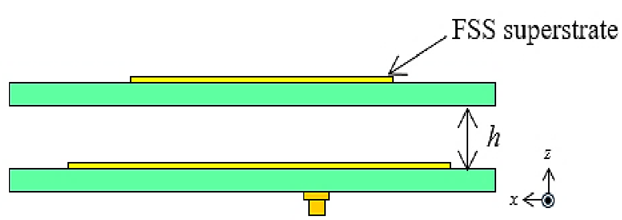

Fig. 7 Air gap between reconfigurable antenna and 1 x 4 passive transmissive FSS

Table 7. Effect of varying the air gap height for h = 6 mm and h = 8 mm

Mode	*h* = 6 mm				*h* = 8 mm			
	Radiation characteristics							
	Tilted angle (°)	Gain (dB)	HPBW (°)	SLL (dB)	Tilted angle (°)	Gain (dB)	HPBW (°)	SLL (dB)
A1	30°	8.06	63.2°	-2.1	32°	7.81	62.5°	-2.2
A2	26°	8.22	62.3°	-8.1	33°	7.2	67.7°	-7.1
A3	28°	7.09	61.9°	-7.6	34°	6.75	66.2°	-6.6
A4	-32°	8.21	60.3°	-1.9	-33°	7.98	60.1°	-2.1
A5	-28°	7.09	61.9°	-7.6	-34°	6.75	66.2°	-6.6
A6	-27°	7.55	62.9°	-8.0	-33°	7.2	67.7°	-7.1
A7	0°	9.63	36.5°	-7.9	0°	9.83	35.9°	-7.5
A8	0°	6.96	83.4°	-18.8	0°	6.29	96.2°	-

Table 7 summarizes the radiation characteristics as the air gap varies from 6 mm to 8 mm in step of 2 mm. At h = 6 mm, the FSS is positioned very close to the strong reactive near-field region of the antenna. Although an improvement is observed relative to the FSS-free case, the imposing smooth and mode-independent transmission-phase gradient.

Increasing the air gap to h = 8 produces a more uniform improvement across all tilted-beam modes. In this configuration, the FSS is sufficiently separated from the antenna to experience a more uniform field distribution while maintaining strong coupling. As a result, the combined phase gradient across the effective aperture becomes more linear, leading to consistent beam tilts of approximately ±32° to ±34° for tilted-beam modes A1-A6, representing enhancements of approximately 4°-6° over the baseline antenna. Meanwhile, the gain remains comparable (≈ 6.7-8.0 dBi), and the HPBWs are maintained between 60.1° and 67.7° range. In addition, the SLL of the tilted modes improve to approximately -6.6 to -7.1 dB, indicating enhanced wavefront coherence and reduce radiation leakage into undesired directions. This simultaneous achievement of increased beam tilt angle, stable gain and HPBW, and improved sidelobe suppression indicates that air gap height of h = 8 provides an optimal balance between antenna-FSS coupling and phase-distribution uniformity, thereby maximizing the effectiveness of the beam steering mechanism.

As summarized in Table 8, further increasing the air gap height to h = 10 mm and h = 12 mm leads to larger beam tilt angles for tilted-beam modes (A1 - A6). For example, the A3 tilted-beam mode configuration achieves a tilted beam angle of 39° at h = 10 mm and 42° at h = 12 mm, compared with 29° for the antenna without FSS. Similar trends are observed for the other tilted beam modes, indicating that a larger antenna-FSS separation can further strengthen the effective phase gradient responsible for beam steering.

Despite the increased beam tilt capability, the overall radiation performance becomes less stable as the air gap height increases. This effect is particularly evident in the broadside operating modes. For example, the A8 mode (all parasitic elements ON), which ideally radiates in the broadside direction (0°), shifts to -13° and -21° at h = 10 mm and h = 12 mm, respectively. Simultaneously, the HPBW increases substantially from 90.5° for the antenna without FSS to 107.5° (h = 10 mm) and 114.5° h = 12 mm), while the gain decreases to 5.81 dBi and 5.64 dBi.

Based on these observations, the air gap study confirms that h = 8 mm provides the optimum air gap height for the proposed FSS-assisted reconfigurable antenna as it provides the most balanced trade-off between beam tilt enhancement, gain preservation, beamwidth control, sidelobe suppression and radiation pattern stability.

Table 8. Effect of varying the air gap height for h = 10 mm and h = 12 mm

Mode	*h* = 10 mm				*h* = 12 mm			
	Radiation characteristics							
	Tilted angle (°)	Gain (dB)	HPBW (°)	SLL (dB)	Tilted angle (°)	Gain (dB)	HPBW (°)	SLL (dB)
A1	33°	7.64	61.9°	-2.3	33°	7.51	61.8°	-2.3
A2	36°	7.75	66.5°	-6.0	39°	7.72	65.8°	-5.4
A3	39°	6.66	67.3°	-5.8	42°	6.74	65.8°	-2.2
A4	-34°	7.87	60.0°	-2.3	-34°	7.78	60.1°	-2.5
A5	-39°	6.66	67.3°	-5.8	-42°	6.74	65.8°	-5.3
A6	-38°	7.12	68.0°	-6.3	-41°	7.18	66.0°	-5.8
A7	0°	9.95	35.2°	-7.0°	0°	10	34.9°	-6.7
A8	-13°	5.81	107.5°	-	-21°	5.64	114.5°	-

6. Results and Discussion

To experimentally verify the simulated beam-tilt enhancement achieved through the transmissive FSS superstrate, a prototype of the optimized configuration parasitic-via reconfigurable antenna integrated with a 1×4 transmissive FSS at an air gap, h of 8 mm, was fabricated and measured. Figure 8 (a) and (b) shows the antenna's structure after soldering with RF components and integrate with 1×4 transmissive FSS, respectively. Accurate via drilling, diode placement and FSS alignment were ensured to minimize structural deviations that could affect beam tilt symmetry and resonance stability.

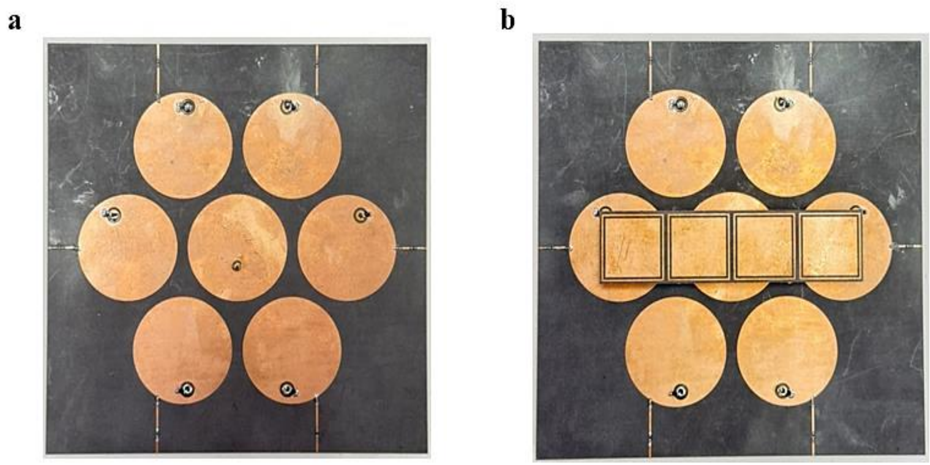

Fig. 8 Prototype of (a) Reconfigurable antenna, and (b) Integrated 1 × 4 FSS with reconfigurable antenna.

The fabricated prototype was experimentally evaluated to characterize its far field radiation characteristics. Figure 9 shows the measurements were conducted in an anechoic chamber using an Over-the-Air (OTA) setup. A standard gain horn antenna used as the transmitting antenna, while the fabricated prototype antenna served as the Antenna Under Test (AUT).

The AUT was placed on a motorized azimuth positioner and rotated through a full 360° to measure the H-plane radiation pattern at 3.5 GHz frequency. For all eight switching configurations (A1 - A8), the respective diode bias states were activated, and the measured far field data were normalized to extract the gain, main beam direction and overall radiation pattern parameters.

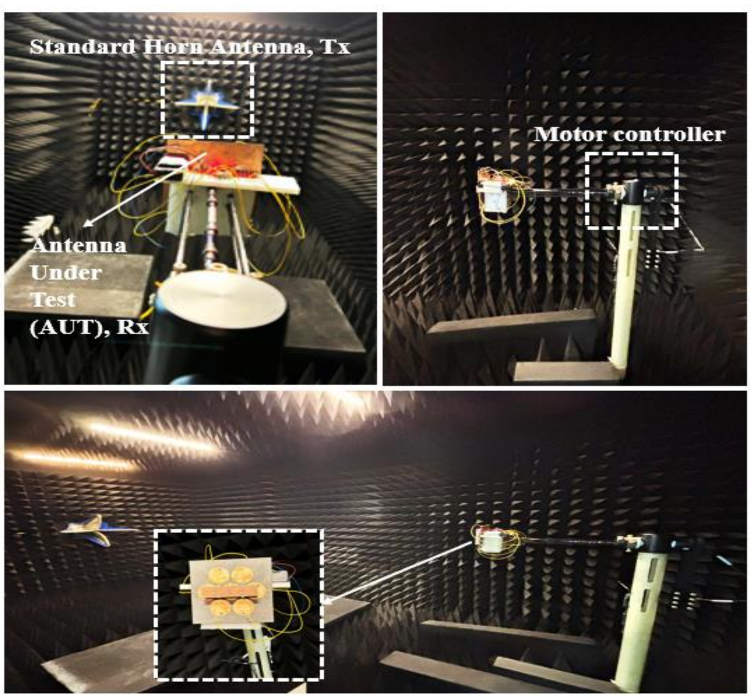

Fig. 9 Measurement radiation pattern setup in anechoic chamber

Figure 10 compares the simulated and measured radiation patterns across A1-A6 switching configurations for the beam tilted modes. The measured main beams clearly tilt toward the intended azimuth sectors dictated by the OFF parasitic pair, confirming that the director-reflector concept remains valid after fabrication and integration of the FSS. The measured tilt magnitude of +32° to +34° for A1-A3 and -33° to -34° for A4-A6 show good agreement with the simulations results and demonstrates an improvement over the baseline parasitic only tilt range of ±24° to ±29°. This improvement is attributed to the passive transmissive FSS, which modifies the transmitted phase distribution above the antenna and strengthens the lateral phase gradient established by the switched parasitic elements. Unlike active FSS and reconfigurable PRS techniques discussed in Table 1, the proposed passive FSS enhances the existing beam steering mechanism without requiring additional active switching or biasing circuits.

Moreover, the measured gains of the tilted beam modes remain relatively stable, ranging from 6.75 to 7.98 dBi, indicating that beam tilt enhancement is achieved without significant degradation in radiation performance.

The corresponding HPBW values are maintain within 60° - 68°, demonstrating that the increased beam tilt does not result in excessive beam broadening. In addition, the measured radiation efficiencies remain high, ranging from 87% to 89%, confirming that integration of the biasing circuit and FSS introduces minimal additional loss.

Figure 11 compares the simulated and measured broadside radiation patterns for switching modes A7 and A8. The measured main beam remains at 0°, validating the preservation of radiation symmetry in the non-steering states. Among these modes, A7 achieves a higher gain of 9.83 dBi and a narrower HPBW of 36°, whereas modes A8 exhibit a lower gain of 6.29 dBi and a broader HPBW of 96°. This difference indicates that the aperture-field distribution produced by the parasitic element configuration in A7 is more favorable for broadside radiation than that in A8. Overall, the measured results validate the proposed design, demonstrating that the passive transmissive FSS enhances the beam steering capability while preserving satisfactory gain, beamwidth and radiation efficiency. The measured radiation characteristics are summarized in Table 9.

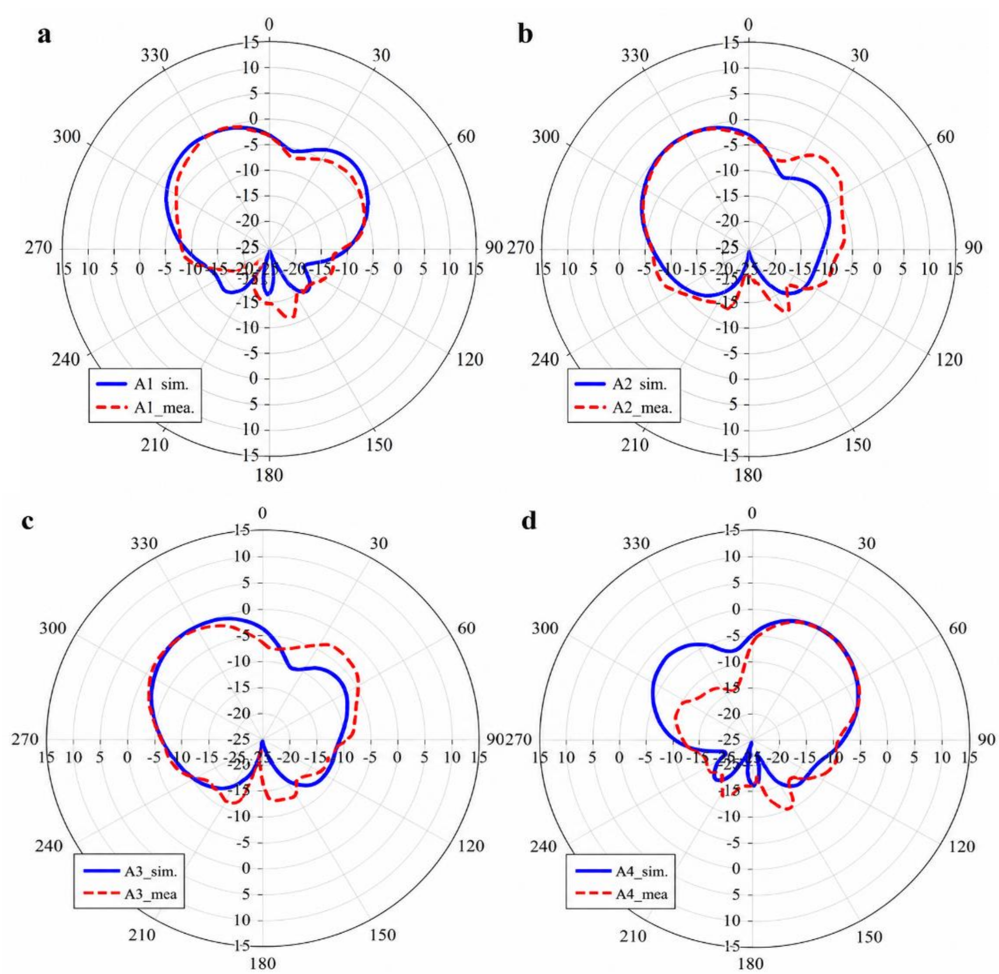

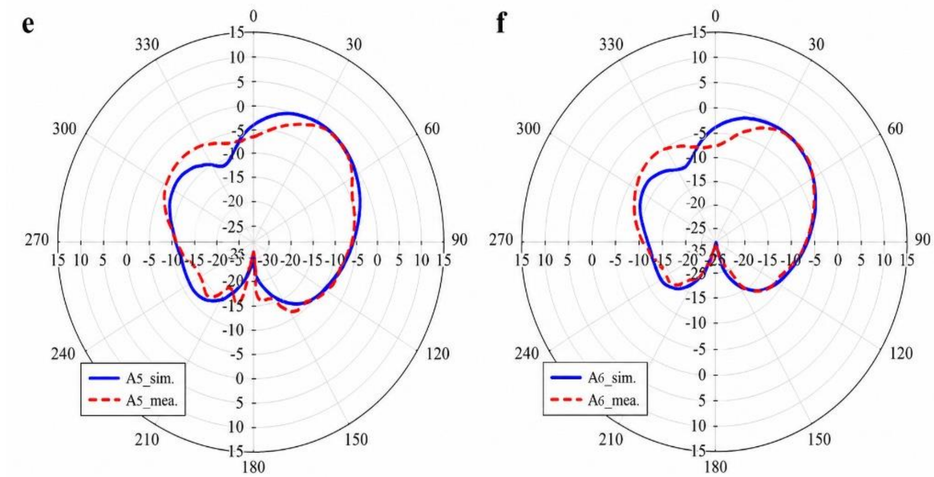

Fig. 10 Comparison between simulated and measured radiation pattern for switching configurations (a) A1, (b) A2, (c) A3, (d) A4, (e) A5, and (f) A6.

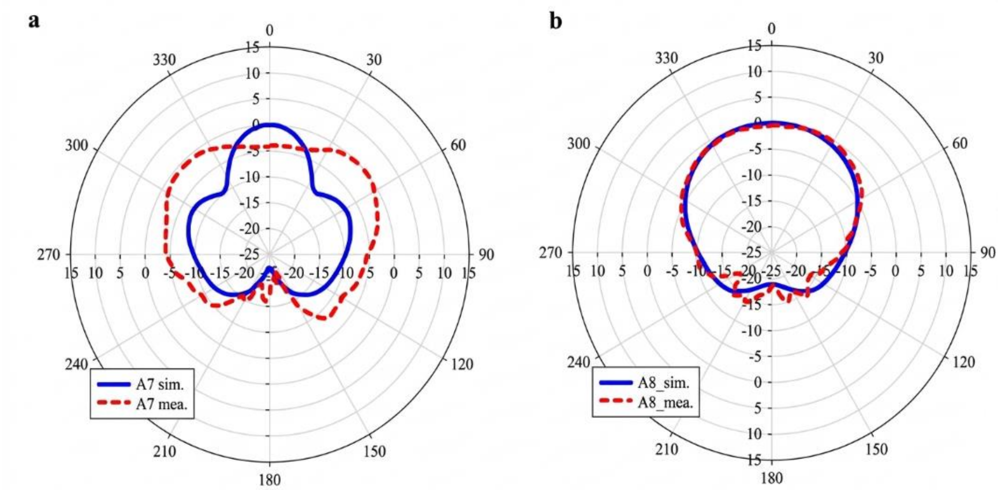

Fig. 11 Comparison between simulated and measured radiation pattern for switching configurations (a) A7, and (b) A8.

Table 9. Measured radiation characteristics of an integrated 1 × 4 FSS array with reconfigurable antenna

Radiation Characteristics	Switching configuration							
	A1	**A2**	**A3**	**A4**	**A5**	**A6**	**A7**	**A8**
Tilted angle (°)	32°	33°	34°	-33°	-34°	-33°	0°	0°
Gain (dB)	7.81	7.2	6.75	7.98	6.75	7.2	9.83	6.29
HPBW (°)	63°	68°	66°	60°	66°	68°	36°	96°
Radiation efficiency (%)	88	87	87	89	87	87	87	89

Figure 12 compares the simulated and measured reflection coefficients, |S11|, for all switching configurations. Overall, simulation and measurement show good agreement, confirming that the fabricated prototype maintains stable impedance matching across all switching configurations.

The measured resonant frequencies range from 3.512 to 3.54 GHz, slightly shifted relative to the simulated frequencies of 3.5 - 3.52 GHz but still consistently resonates within the intended 3.5 GHz band. The measured |S11| are slightly less than the simulated due to practical losses and fabrication imperfections. Nevertheless, all switching configurations satisfy the impedance matching criteria of |S11| < -10 dB. These results show that the integration of the transmissive FSS and biasing network does not significantly affect the input impedance of the antenna.

The proposed antenna operates within 3.4 - 3.6 GHz frequency allocation designated by the Malaysian Communications and Multimedia Commission (MCMC) for sub-6 GHz 5G deployment, confirming its suitability for 5G applications in Malaysia [24].

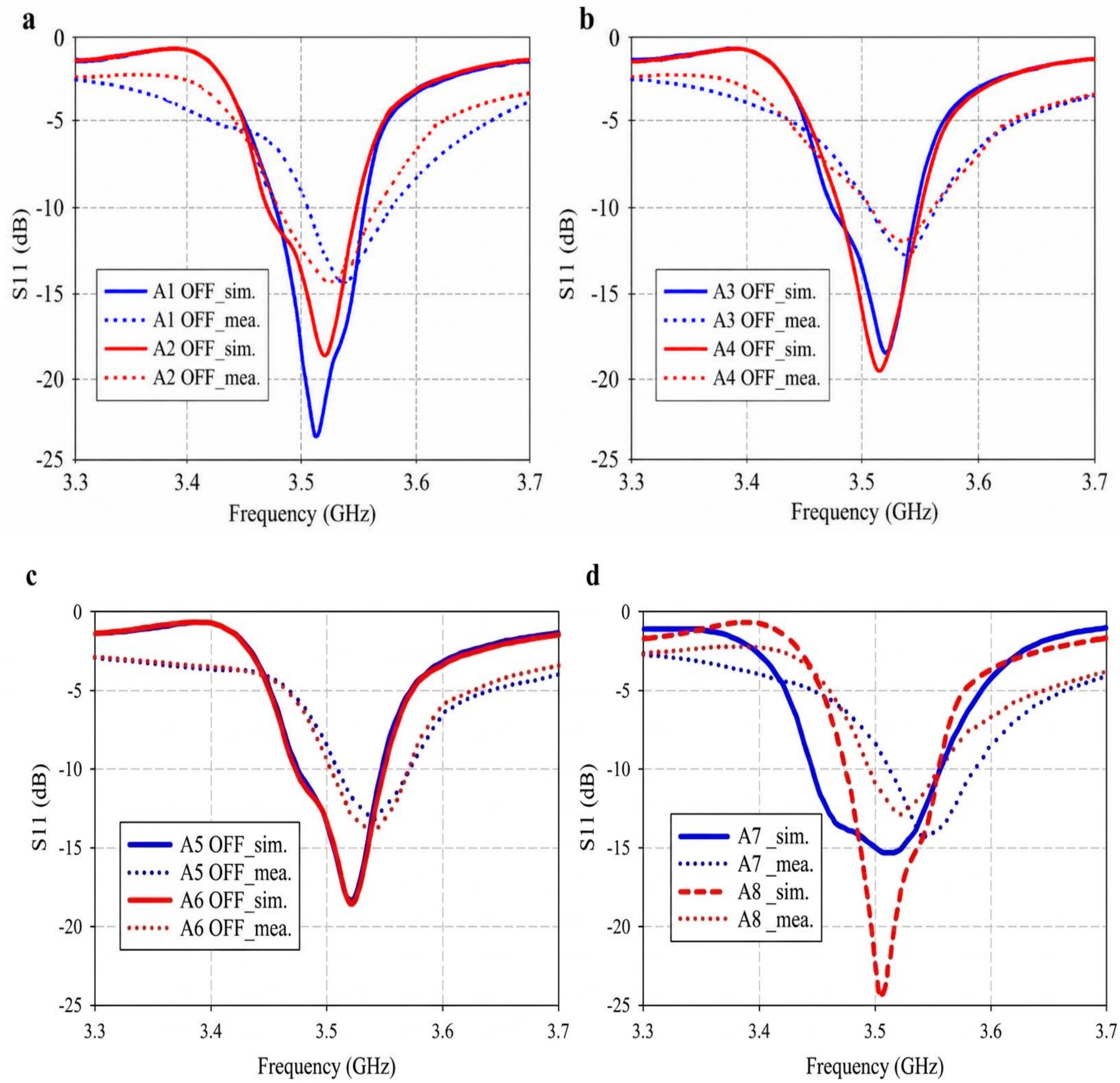

Fig. 12 Comparison between simulated and measured reflection coefficient $|S_{11}|$ for switching configurations, (a) A1 and A2, (b) A3 and A4, (c) A5 and A6, (d) A7 and A8.

7. Conclusion

This work has demonstrated a novel 360° beam-reconfigurable parasitic-via circular patch antenna enhanced using a passive transmissive FSS superstrate for the 3.5 GHz sub-6 GHz band. By integrating an optimized 1×4 transmissive FSS at an 8 mm air gap, the effective lateral phase gradient was reinforced, resulting in a beam tilt angle improvement from ±24°-29° to ±32°-34° without compromising gain, HPBW, or radiation efficiency. The strong agreement between simulated and measured responses verifies modelling accuracy and confirms that passive FSS-assisted field shaping is a viable approach for compact and energy-efficient beam steering in future sub-6 GHz 5G deployments.

Funding statement

This work was financially supported by Universiti Teknologi MARA (UiTM) under the incentives of 'Pembayaran Yuran Penerbitan Artikel (PYPA)'.

Acknowledgments

The authors would like to thank the Antenna Research Centre (ARC), Faculty of Electrical Engineering, Universiti Teknologi MARA, Shah Alam, Selangor and Centre of Foundation Studies, Campus Dengkil, for their valuable support.

References

[1] Quoc Hung Dang et al., "A Frequency-Reconfigurable Wearable Textile Antenna with One-Octave Tuning Range," *IEEE Transactions on Antennas and Propagation*, vol. 69, no. 12, pp. 8080-8089, 2021. [CrossRef] [Google Scholar] [Publisher Link]

[2] Sangeetha Subbaraj et al., "A Compact Frequency-Reconfigurable Antenna with Independent Tuning for Hand-Held Wireless Devices," *IEEE Transactions on Antennas and Propagation*, vol. 68, no. 2, pp. 1151-1154, 2020. [CrossRef] [Google Scholar] [Publisher Link]

[3] Ismail Ben Mabrouk et al., "A Novel Design of Radiation Pattern-Reconfigurable Antenna System for Millimeter-Wave 5G Applications," *IEEE Transactions on Antennas and Propagation*, vol. 68, no. 4, pp. 2585-2592, 2020. [CrossRef] [Google Scholar] [Publisher Link]

[4] Jeen-Sheen Row, and Yu-Hsin Wu, "Pattern Reconfigurable Slotted-Patch Array," *IEEE Transactions on Antennas and Propagation*, vol. 66, no. 3, pp. 1580-1583, 2018. [CrossRef] [Google Scholar] [Publisher Link]

[5] Ka Ming Mak et al., "Polarization Reconfigurable Circular Patch Antenna With a C-Shaped," *IEEE Trans Antenna Propagation*, vol. 65, no. 3, pp. 1388-1392, 2017. [CrossRef] [Google Scholar] [Publisher Link]

[6] Jian Ren et al., "Radiation Pattern and Polarization Reconfigurable Antenna using Dielectric Liquid," *IEEE Transactions on Antennas and Propagation*, vol. 68, no. 12, pp. 8174-8179, 2020. [CrossRef] [Google Scholar] [Publisher Link]

[7] Ruolei Xu, and Zhi Ning Chen, "A Compact Beamsteering Metasurface Lens Array Antenna with Low-Cost Phased Array," *IEEE Transactions on Antennas and Propagation*, vol. 69, no. 4, pp. 1992-2002, 2021. [CrossRef] [Google Scholar] [Publisher Link]

[8] Shenario Ezhil Valavan et al., "Dual-Band Wide-Angle Scanning Planar Phased Array in X/Ku-Bands," *IEEE Transactions on Antennas and Propagation*, vol. 62, no. 5, pp. 2514-2521, 2014. [CrossRef] [Google Scholar] [Publisher Link]

[9] You-Feng Cheng et al., "2-D Planar Wide-Angle Scanning-Phased Array based on Wide-Beam Elements," *IEEE Antennas and Wireless Propagation Letters*, vol. 16, pp. 876-879, 2017. [CrossRef] [Google Scholar] [Publisher Link]

[10] Liwen Jing, Meng Li, and Ross Murch, "Compact Pattern Reconfigurable Pixel Antenna with Diagonal Pixel Connections," *IEEE Transactions on Antennas and Propagation*, vol. 70, no. 10, pp. 8951-8961, 2022. [CrossRef] [Google Scholar] [Publisher Link]

[11] Devakumaran Subramaniam et al., "A Stacked Planar Antenna with Switchable Small Grid Pixel Structure for Directive High Beam Steering Broadside Radiation," *International Journal of Engineering and Technology*, vol. 7, no. 2.5, pp. 122-127, 2018. [CrossRef] [Google Scholar] [Publisher Link]

[12] Md. Asaduzzaman Towfiq et al., "A Reconfigurable Antenna with Beam Steering and Beamwidth Variability for Wireless Communications," *IEEE Transactions on Antennas and Propagation*, vol. 66, no.10, pp. 5052-5063, 2018. [CrossRef] [Google Scholar] [Publisher Link]

[13] Parisa Lotfi, Saber Soltani, and Ross D. Murch, "Printed Endfire Beam-Steerable Pixel Antenna," *IEEE Transactions on Antennas and Propagation*, vol. 65, no. 8, pp. 3913-3923, 2017. [CrossRef] [Google Scholar] [Publisher Link]

[14] Fan Jiang et al., "Pixel Antenna Optimization using *N*-Port Characteristic Mode Analysis," *IEEE Transactions on Antennas and Propagation*, vol. 68, no. 5, pp. 3336-3347, 2020. [CrossRef] [Google Scholar] [Publisher Link]

[15] Yujie Zhang et al., "A Highly Pattern-Reconfigurable Planar Antenna with 360° Single- and Multi-Beam Steering," *IEEE Transactions on Antennas and Propagation*, vol. 70, no. 8, pp. 6490-6504, 2022. [CrossRef] [Google Scholar] [Publisher Link]

[16] M.S. Alam, and A.M. Abbosh, "Wideband Pattern-Reconfigurable Antenna using Pair of Radial Radiators on Truncated Ground with Switchable Director and Reflector," *IEEE Antennas and Wireless Propagation Letters*, vol. 16, pp. 24-28, 2017. [CrossRef] [Google Scholar] [Publisher Link]

[17] Shu-Lin Chen et al., "Pattern-Reconfigurable Antenna with Five Switchable Beams in Elevation Plane," *IEEE Antennas and Wireless Propagation Letters*, vol. 17, no. 3, pp. 454-457, 2018. [CrossRef] [Google Scholar] [Publisher Link]

[18] Thennarasan Sabapathy et al., "Electronically Reconfigurable Beam Steering Antenna using Embedded Rf Pin based Parasitic Arrays (ERPPA)," *Progress in Electromagnetics Research*, vol. 149, pp. 241-261, 2013. [CrossRef] [Google Scholar] [Publisher Link]

[19] Sagiru Gaya et al., "Pattern Reconfigurable Yagi-Uda Antenna with Seven Switchable Beams for WiMAX Application," *Microwave and Optical Technology Letters*, vol. 62, no. 3, pp. 1329-1334, 2020. [CrossRef] [Google Scholar] [Publisher Link]

[20] Wenbo Pan et al., "A Beam Steering Horn Antenna using Active Frequency Selective Surface," *IEEE Transactions on Antennas and Propagation*, vol. 61, no. 12, pp. 6218-6223, 2013. [CrossRef] [Google Scholar] [Publisher Link]

[21] Lu-Yang Ji, Zhi-Ya Zhang, and Neng-Wu Liu, "A Two-Dimensional Beam-Steering Partially Reflective Surface (PRS) Antenna using a Reconfigurable FSS Structure," *IEEE Antennas and Wireless Propagation Letters*, vol. 18, no. 6, pp. 1076-1080, 2019. [CrossRef] [Google Scholar] [Publisher Link]

[22] Gowri P et al., "EM Design of Beam Steering Antenna using Active Frequency Selective Surfaces at 24 GHz," *IEEE Wireless Antenna and Microwave Symposium (WAMS)*, Visakhapatnam, India, pp. 1-5, 2024. [CrossRef] [Google Scholar] [Publisher Link]

[23] Abdullah Qayyum et al., "A Novel mmWave Defected Ground Structure based Microstrip Antenna for 5G Cellular Applications," *2020 First International Conference of Smart Systems and Emerging Technologies (SMARTTECH)*, Riyadh, Saudi Arabia, pp. 28-31, 2020. [CrossRef] [Google Scholar] [Publisher Link]

[24] Malaysian Communications and Multimedia Commission, International Institute of Communications, 2022. [Online]. Available: https://www.iicom.org/member/malaysian-communications-and-multimedia-commission-mcmc/